Introduction

1.1 General introduction to nanoparticles

Nobel Laureate Richard Feynman in his visionary lecture “There is plenty of room at the bottom”[1] inspired the concepts for the rapidly exploding research topic of nanotechnology by various research group all over the world. Although the term “nanotechnology” had not appeared on the horizon, Feynman said: “What I want to talk about is the problem of manipulating and controlling things on a small scale… What I have demonstrated is that there is room—that you can decrease the size of things in a practical way… I will not discuss how we are going to do it, but only what is possible in principle… We are not doing it simply because we haven’t yet gotten around to it.” Now-a-days scientists have learnt that the manipulation of atoms, molecules, and clusters on surfaces is feasible and that new fundamental of science governs the properties of nano-objects.

The term “nano” is derived from the Greek word “nanos” for “dwarf”. This etymology, and its placement on the metric scale (1nm = 10^{-9} m), shows that tiny dimensions not visible to naked eye, beyond the normal limits of our observation. The diameter of hair (100 μm) to the buck-minster fullerene (1 nm) shows the variation of diameter of a material (Figure 1.1) [2]. Nanoscale materials are defined as materials having at least one dimension in the 10–100 nm range, in which nanoparticles are the major investigated subjects. The term “nano-particle” (earlier termed small particles) first appeared in the 1980s.[3, 4]

The nanoscience deals with the materials having particle size in nanometer regime and their properties. The interdisciplinary nature with contributions from chemistry, physics, biology, materials sciences, all the way to engineering and medicine is one of the most striking features of the nanosciences when compared to many classical disciplines, and is important for the development of nanotechnological products.

The past few decades have witnessed an exponential growth of activities in the field of nanometer-scale science and technology, driven by the excitement of understanding a new research area and by the potential hope for applications and economic impacts. The synthesis of nanoparticles of different size and shape has received largest activity in the past few years as a result of their peculiar and fascinating properties, and their applications superior to their bulk counterparts. The most successful example is microelectronics, where "smaller" has meant greater performance ever since the invention of integrated circuits which leads to more components per chip, faster operation, lower cost and less power consumption [5].

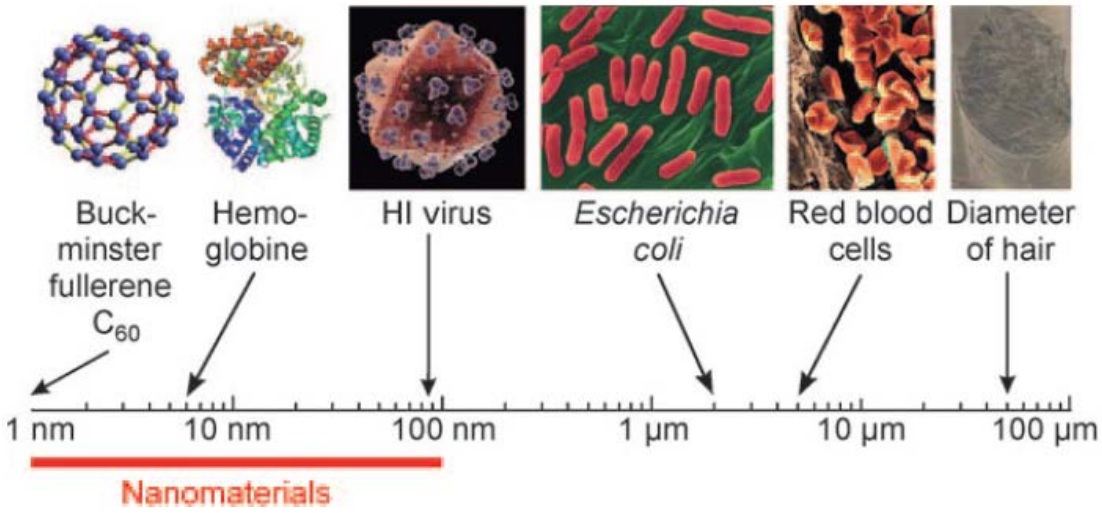

Figure 1.1 Length scale for classifying nanoparticles.[2]

Besides small size, the characteristic feature of nanomaterial is their vast surface area. This concept can be illustrated with Figure 1.2 and table 1. Take a cube with edges 1 cm in length and divide into cubes with edges 1 nm in length. In such a case, the total volume remains same, but the number of individual cubes and their total surface area increases. The surface area of the 10^{21} "nanocubes", at 6000 m^2, amounts roughly the area of a football field (ca. 7000 m^2) created from a single cube of edges 1 cm. Hence the surface area of a material (bulk) increases dramatically when the particle size decrease to nanometer range.

The interest in nanoscale materials is due to fact that new properties are acquired at this length scale and, equally important, that these properties change with their size or shape. The change in the properties of the material at this length scale when compared with the bulk material, results from different causes in different materials. The increase in the surface area of a material is a desired property in the field of catalysis. These nano-materials can be used as catalyst itself or as a catalyst support.

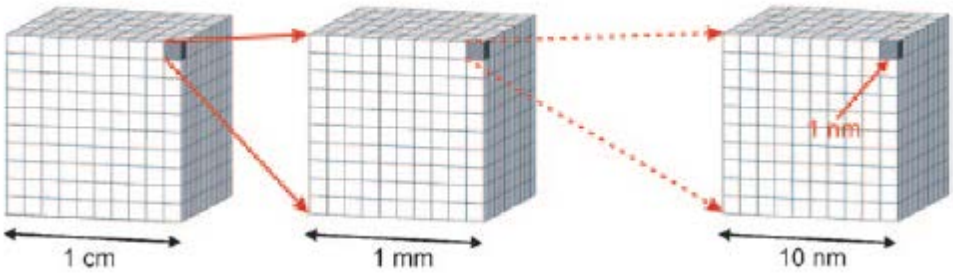

Figure 1.2 Surface area of nanoparticles in a simple model [2].

Table no. 1 Increase of surface area of a cube with decreasing edge size.

Edge length of cubes	*Number of cubes*	*Volume of cubes*	*Surface area of cubes*
1 cm	1	1 cm^3	0.0006 m^2
1 mm	10^3	1 cm^3	0.006 m^2
1 µm	10^{12}	1 cm^3	6 m^2
1 nm	10^{21}	1 cm^3	6000 m^2

Nanoparticles find an important application in heterogeneous catalysis [6]. As the catalytic reaction occurs on the surface, the available catalyst surface area correlates directly with the turnover number of material. In case of noble metals, the advantage of nanoparticles is cost. The heterogeneous catalysis is an example of a major industrial relevance of nanoparticles.

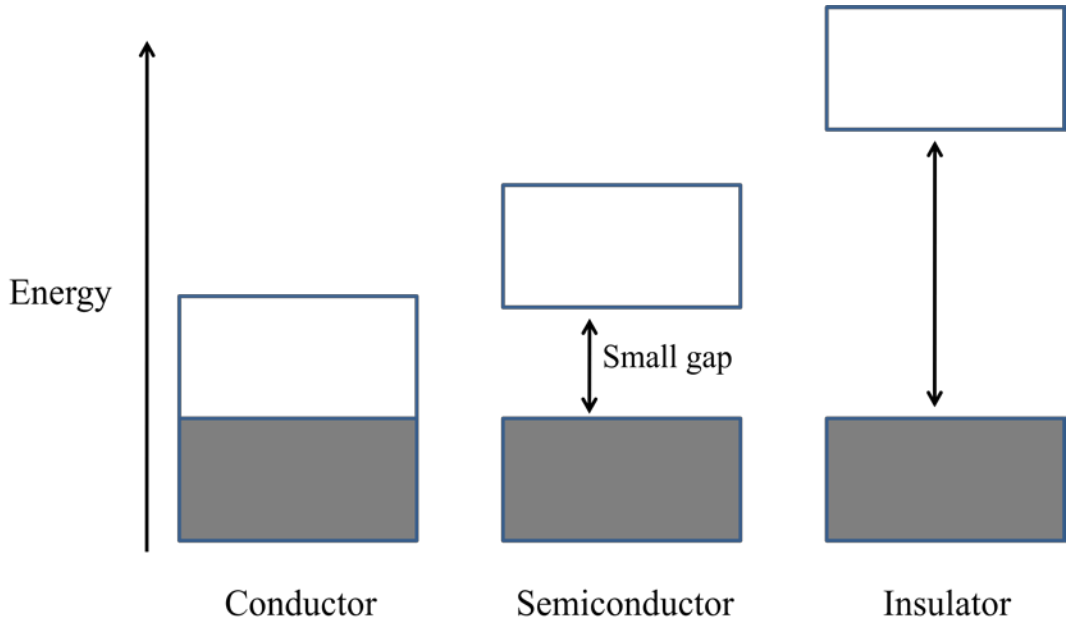

Figure 1.3 Different types of material viz. metal, semiconductors and insulators, on the basis of the overlap or separation between valence band and conduction bands.

Different materials can be classified as metals, semiconductor and insulator based on the differences between the valence band and conduction band, as shown in Figure 1.3.

Semiconductor nanoparticles find applications in nanoelectronics, optoelectronics, photonics sensors, medical diagnostics, catalysis, photocatalysis etc. In most of their potential applications, quality and structure of the surface play the pivotal role in determining their functions.

Another application for nanoparticles is suntan lotion as protection against ultraviolet radiation that has been commercially significant for quite a long time [7]. Suntan lotion contains the TiO_2 or ZnO nanoparticles (diameter 30–80 nm) that can serve as a simple example of the optical transparency of thin layers of nanoparticles when the size of the nanoparticles is well below the wavelength of visible light (380–780 nm) [8]. While a thick layer of suntan lotion appears milky white because of diffuse

multiple scattering at the nanoparticles, a thin layer on the skin is transparent which is no longer visible to the human eye.

1.2 Metal nanoparticles

In case of noble metals, when the particles size are reduced to tens of nanometers, a new strong absorption is observed resulting from the collective oscillation of the electrons in the conduction band from one surface of the particle to the other. This oscillation has a frequency in the visible light range, which is known as the surface plasmon absorption. This strong absorption, giving rise to vivid characteristic color, has been observed and used, since the 17^{th} century. The gold particles, giving rise to a brilliant rose color which have found wide use in stained glass windows of cathedrals throughout Europe and by the Chinese in coloring vases and other ornaments. In transition metal nanoparticles, the decrease in the particle size to the nanometer length scale increases the surface-to-volume ratio, makes them potentially useful in the field of catalysis.

1.3 Semiconductor nanoparticles

In the past few years, a great deal of attention has been directed towards studying the properties of a new class of materials formed from conventional semiconductors. These materials are well known as quantum-confined nanoclusters or quantum dots, are tiny spheres (*OR 1-10 nm* ca. 10-100 Å in diameter) of a conventional semiconductor, such as ZnS, CdS, PbS, etc. Quantum dots (QDs) are confined system, bridging the gap between bulk matter and molecular species, promise to be important in the next-generation nanometer-scale devices [9]. They exhibit optical, electronic and magnetic properties, very different from that observed for the bulk solid semiconductor. These differences arise from quantum confinement effects due to the reduction of band structure into discrete quantum levels as a result of the limited size of the particle and hence the band gap energy value increases (figure 1.4).

An interesting behavior arises in these materials due to the confinement of optically excited electron-hole pairs by the crystallite boundary. The basic explanation of this phenomenon, known as the quantum size effect, was provided early in the investigation of these materials, a detailed understanding required the advent of high-quality colloidal nanocrystals, which were uniform in size, shape, crystallinity, and surface passivation.

In case of semiconductor nanoparticles, it results from the further confinement of the electronic motion to a length scale that is comparable to or smaller than the length scale characterizing the electronic motion in bulk semiconducting material (called the electron Bohr radius, which is usually a few nanometers). Having the ability to adjust the band gap can be extremely useful for developing chalcogenides nanoparticles with novel optical properties and applications.

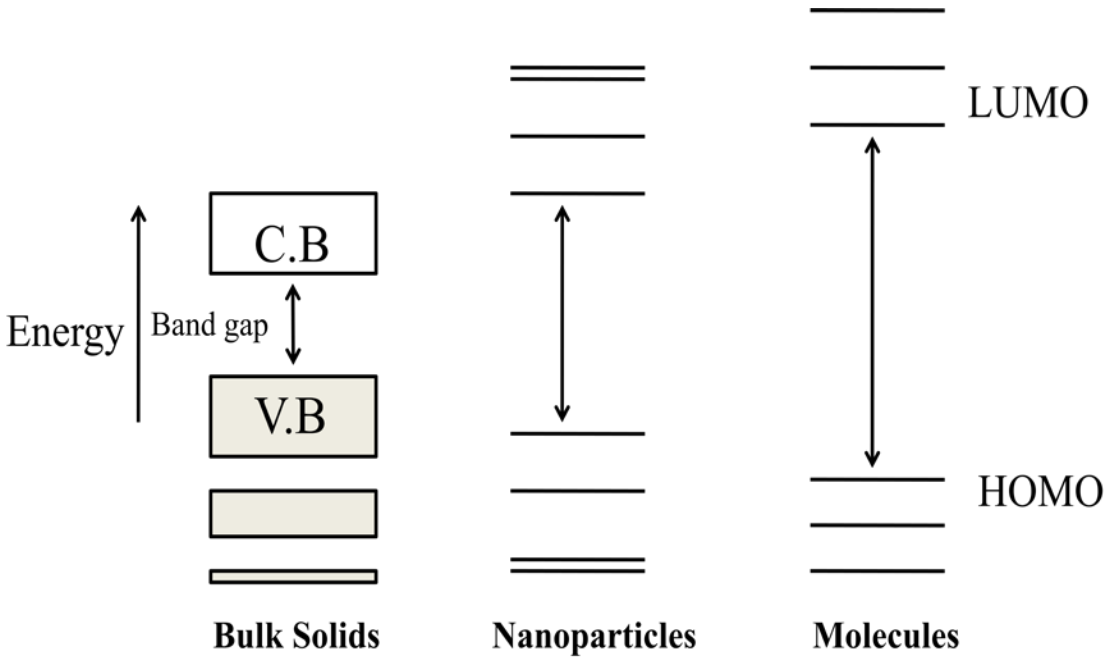

Figure 1.4 Diagram of increasing band gap with the particle size.

1.4 II-VI semiconductor terminology:

The II-VI semiconductor is a common terminology for the compound formed with the IIB group and VI group elements as shown in Figure 1.4. The IIB group represents the elements like Zn, Cd and Hg and the VI group represents the elements like O, S, Se, Te and Po. The compounds of group VI are also knowns as chalcogenides.

1.5 Quantum confinement effect

A macrocrystalline semiconductor which is free of defects, consist of three-dimensional networks of ordered atoms. The translational periodicity of the crystal results in a special form on the electronic wave functions. A Bloch type wave function (eq 1) can be used to describe an electron in the periodic potential field of a crystal, where u(r) represents a Bloch function modulating the plane wave-(kr) of wave vector k.

$$\psi(\mathrm{r}) = \phi(kr)u(r) \quad \text{.....(1)}$$

In a bulk semiconductor, large number of atoms leads to the generation of sets of molecular orbitals with very similar energies, which form a continuum or band. The lower energy levels, or valence band, are filled with electrons, while the conduction band consisting of the higher energy levels is unoccupied at 0 K. These two bands are separated by an energy gap (Eg) and the magnitude of which is a characteristic property of the bulk macrocrystalline material at a specific temperature. Materials normally are considered as semiconductors, which typically exhibit band gaps energy in the range 0.3-3.8 eV.

The band gap is simply calculated from the excitonic absorption peak by using the equation,

$$E_g = \left(\frac{hc}{\lambda}\right) \quad \text{..... (2)}$$

where *h* is the Planck's constant, *c* is velocity of light, and λ is the peak wavelength.

There are two fundamental factors related to the size of nanocrystals and change their behavior drastically from the corresponding macrocrystalline/bulk material. The first is the high large surface/volume ratio, both the physical and chemical properties of the semiconductor are affected by this parameter. The second is the particle size which determines the electronic and physical properties of the material. Mie's theory describes the absorption and scattering of incident light from larger colloidal particles. However, the blue shift in the absorption edge of nanocrystalline semiconductors with decrease in [10], particle size cannot be explained by classical theory [11-14]. These size dependent optical properties are examples of the quantization effect which occurs [11] when the size of the nanoparticles is smaller than the bulk-exciton Bohr radius, a_B (eq 3), of the semiconductor.

$$a_B = \hbar^2 \varepsilon / e^2 [\frac{1}{m_{e^*}} + \frac{1}{m_{h^*}}] \quad \text{..... (3)}$$

Equation 4 defines, for a spherical crystallite of radius R, it is the region of intermediate character between that of a "molecule" and that of the bulk material (where l is the lattice spacing).

$$I \ll R \leq a_B \quad \text{..... (4)}$$

In semiconductor nanocrystallites the charge carriers are confined within three dimensions. Hence, the wave function in eq 1 has to satisfy the boundary conditions, in the case of ideal quantum confinement

$$\psi(r \geq R) = 0 \quad \text{..... (5)}$$

In case of nanoparticles the electron and hole are closer together than in the macrocrystalline material, and as such the Coulombic interaction between electron and hole cannot be neglected; they have higher kinetic energy than in the macrocrystalline material.

Brus et al. showed [10,12,13] for CdE (E) S or Se) nanocrystallites (on the basis of the effective mass approximation) that the size dependence on the energy of the first electronic transition of the exciton (or the band gap shift with respect to the typical bulk value) can be approximately calculated using

$$\Delta E \cong \frac{\hbar^2 \Pi^2}{2R^2}\left[\frac{1}{m_e{}^*} + \frac{1}{m_h{}^*}\right] - \frac{1.8e^2}{\varepsilon R} \qquad \ldots\ldots\ldots\ldots\ldots\ldots\ldots\ldots\ldots\ldots\ldots\ldots\ldots\ldots (6)$$

Equation 6 which is an analytical approximation for the first electronic transition of an exciton, where m_e^* = effective mass of electron, m_h^* = effective mass of hole, ε = dielectric constant of the material, ε_0 = permittivity of free space and h = Planck's constant.

1.6 Different Morphologies

Size and shape are the two crucial geometrical parameters that determine novel phenomena at nanoscale. Figure 1.5 illustrates the basic geometrical structures of inorganic nanocrystals: zero-dimensional (0D) isotropic spheres, cubes, and polyhedrons; 1D rods and wires; 2D discs, prisms, and plates and complex structure are tetrapods, flower and star like. These nanostructures with well define shapes are suitable for functional applications. One-dimensional ZnS nanoparticles are well suited for solid lasers and circuits for future devices.

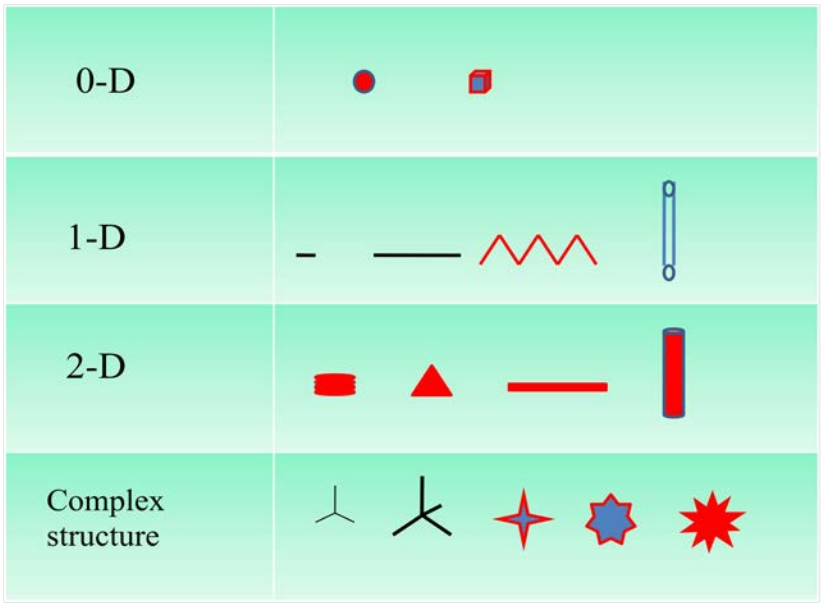

Figure 1.5 Basic structures of inorganic nanocrystals: 0D spheres and cubes; 1D rods and wires; 2D discs, prisms, and plates and complex structure like tripods, tetrapods, star-like and flowers like.

1.7 Stability of nanoparticles

Thermodynamically, nanoparticles are unstable against an unlimited growth, and have tendency to form large clusters or agglomerates. The surface has to be passivated by proper molecules to arrest their growth, resulting in repulsive interactions among the particles. The thermodynamic stability also changes dramatically with size. In various nanomaterials the depression of the melting point has been reported [15]. Also, structural transformations have been demonstrated to take place in nanomaterials at relatively lower temperatures.[16] In an earlier report, it had been shown that, under certain conditions, nanoparticles of CdS both in the wurtzite and sphalerite structures simultaneously existed at low temperature.[17]

1.8 Synthetic procedure

The synthetic procedure can be classified into two types based on the starting approach i.e. beginning with molecules or bulk material Figure 1.6.

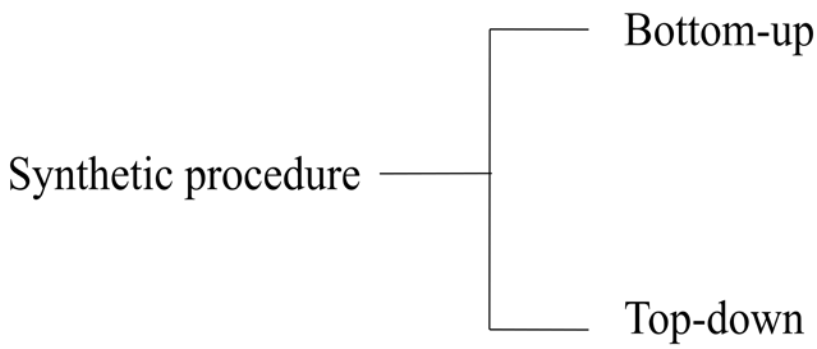

Figure 1.6 Classification of synthesis procedure of nanoparticles.

In bottom-up approach or ‘self-assembly’ (assembling particles synthesized in solution) is a process universal in nature, atoms and molecules are assembled from molecular levels so as to have nanomaterials of desired size and shape by controlled reaction parameters. Wet chemical synthesis is the most energy efficient ‘bottom up’ technique for the synthesis. In top down approach reverse is the case. The conventional approach involves chemical or physical attrition from bulk into objects of desired sizes and shapes (e.g. lithography, mechanical milling, ion implantation, etc.), and is known as the ‘top-down’ approach.

Size and shape of nanoparticles can be tuned by careful control of synthesis parameters like reaction temperature, solvent system, concentration of capping agent and functional groups present in it, pH of the reaction medium, etc.

The physical properties and applications of nanostructured materials are heavily dependent upon how they are prepared. A large variety of methods are employed, including microwave method [18], hydrothermal method [19], sol-gel method [20], solvothermal method [21], spray-pyrolysis method [22], chemical vapour deposition (CVD) etc [23].

The wet chemical routes provide the better control over size and morphology and are more facile and promising for industrial-scale preparation. However, relatively

simple, mild and low-cost synthesis methods are still on the way and need to be further sought for.

1.9 Template directed Synthesis

Any organic or inorganic materials such as polystyrene and silica latex spheres [24],[25], liquid crystals [26], surfactant vesicles [27], polymer micelles [28], microemulsion droplets [29], etc are used as templates. Such templates, after synthesis, can be recovered or calcinated resulting in nanoparticles having morphology and size of the host's cavity. In case of soft matter like reverse micelle, the shape and size can be controlled by tuning the parameters such as water to surfactant ratio (ω), pH, temperature etc.

Particle size and agglomeration behavior can be controlled effectively in the liquid phase synthesis. The reactive surfaces can be stabilized with capping agents immediately after nucleation (Figure 1.7). The capping agent is a key parameter when preparing nanomaterials, the capping agent can be thought of primarily as a stabilising agent, providing colloidal stability, stopping uncontrolled growth and agglomeration. The growth kinetics of different crystal facets can be tuned by selective adhesion of surfactant molecules and tailored NC shape from nearly spherical to highly anisotropic can be obtained [30].

The capping ligands control various parameters such as the rate of growth, particle morphology, reaction pathways and the particle size distribution during the chemical reaction. The electronic structure of the passivating ligands contributes to the overall electronic and optical profile of the nanomaterial, blocking surface states and hence affecting emission yields. The most successful example of the importance of a capping agent is the CdTe/thiol system, where the energy levels of the thiol inhibit hole trapping and the resulting material is extremely luminescent without the requirement of further inorganic shells or prolonged processing [31]. Some capping agents are chemically labile, and can react with the nanoparticles producing new

materials, for example CoPd sulfide ‘nanoacorns’ [32]. In this case, reduction of cobalt and palladium precursors in the presence of 1-octanethiol resulted in phase-segregated nanomaterials, with an elongated Co_9S_8 section joined with a PdS_2 section.

Surface modification of individual nanoparticles by an inorganic or organic material with a wider band gap contributes to (a) surface passivation to reduce surface trap sites for non-radiative transition and (b) quantum confinement effects to promote the recombination of electron-hole pairs in a limited nano-space [33].

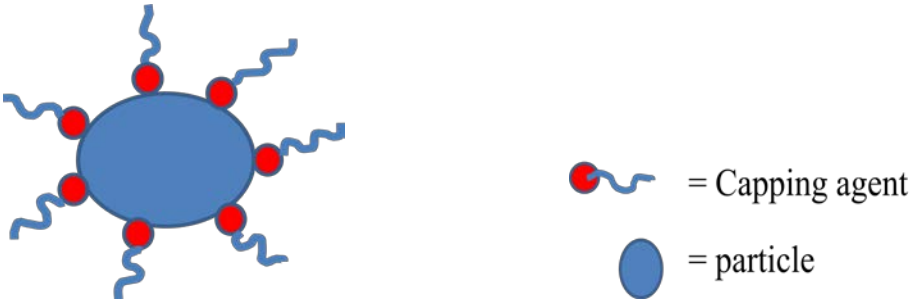

Figure 1.7 Role of a capping agent during the synthesis of nanoparticles.

1.10 Different types of ligands used as capping agents during synthesis.

Tri-n-octylphosphine oxide (TOPO)

The advantages of using TOPO (Figure 1.8) as a surfactant, solvent and capping agent include the high boiling point, allowing reactions to proceed routinely at 350 °C facilitating high temperature precursor decomposition and annealing which is not available in aqueous routes. Also, the compatibility with organic solvents allows a complete inert reaction environment and hence air sensitive precursors can be used. The long alkyl chains impart solubility to the quantum dots and allow the material to be manipulated like a common organic reagent (although the solvents used must possess a significantly high dielectric constant to overcome the van-der Waals

attraction between the colloidal particles) during the reaction. The ligand shell in case of most of semiconductors, able to stand several rounds of dispersion/ precipitation before losing any degree of solubility as the surfactant is gradually removed. The steric properties of the alkyl groups also affect particle growth, controlling shape and morphology [34, 35].

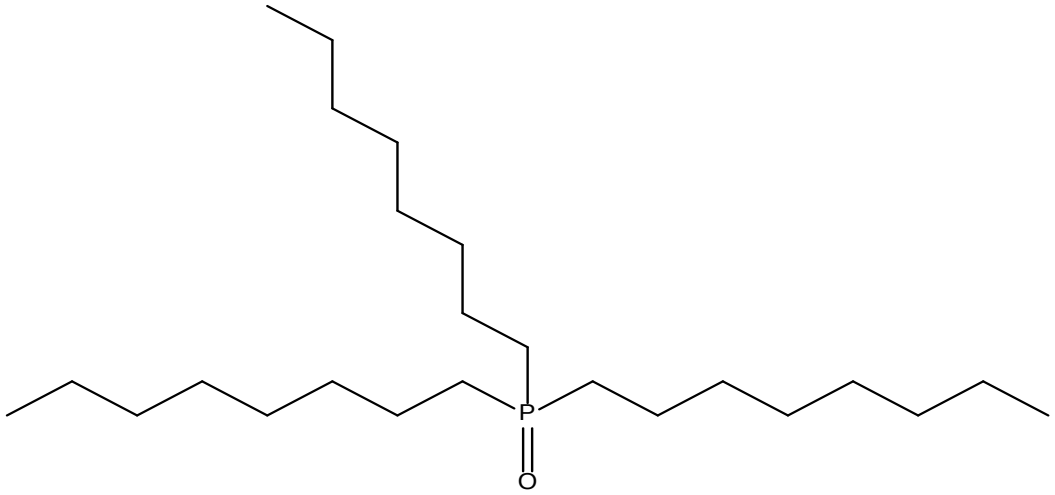

Figure 1.8. Molecular structure of Trioctylphosphine oxide (TOPO).

Tri-n-octylphosphine (TOP)

During the preparation of TOPO capped CdSe nanocrystals, tri-n-octylphosphine (TOP) (Figure 1.9) is also routinely used as both a surfactant and selenium-delivery solvent when in the form of a trioctylphosphine selenide (TOPSe) solution. Trioctylphosphine is generally thought to coordinate to the surface of the particles along side TOPO, via the selenium sites, supplying a more surface passivation. Furthermore, the conventional QDs synthesis route uses organic solvents such as tri-n-octylphosphine/trin-octylphosphine oxide (TOP/TOPO) and organometallic precursors that are environmentally hazardous [36], which is a major drawback of this ligand.

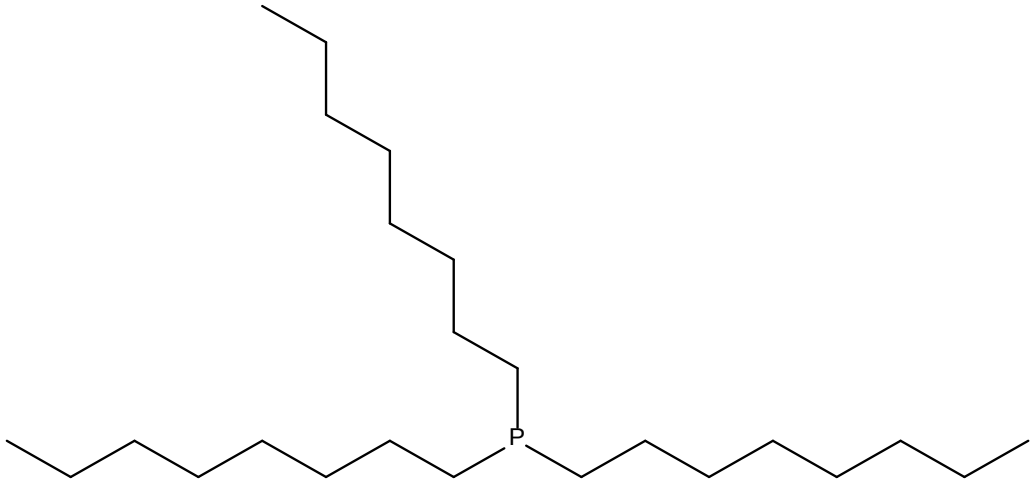

Figure 1.9. Molecular structure of Trioctylphosphine (TOP).

TOPO and TOP, however, are not ideal solvents as upon heating TOPO above 300 °C is known to induce decomposition,[37] the product of which is unidentified but is known to luminesce (albeit weakly). This decomposition product emission can in some cases be mistaken for semiconductor emission, especially when the parent semiconductor exhibits a low emission quantum yield [38].

Amines

For II–VI based semiconducting systems long chain amines are found to be more suitable surfactants. CdSe nanoparticles prepared using long chain primary amines are generally found to have emission quantum yields of 60% without the need for an inorganic shell [39,40]. This has been attributed to the closer packing of the ligands on the surface of nanoparticle and the etching of surface defects,[41] whilst amines have also been shown to contribute to the oxygen etching process [42]. The use of amines as capping agents on CdSe particles has also been shown to result in a surface reconstruction, [43] specifically a lattice contraction during growth of nanoparticles, which may contribute to the elevated emission. Eg. dodecylamine and oleylamine (Figure 1.10, 1.11) [44].

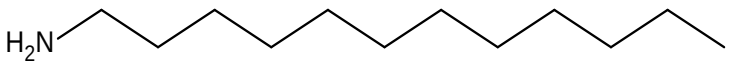

Figure 1.10 Molecular structure of Dodecylamine.

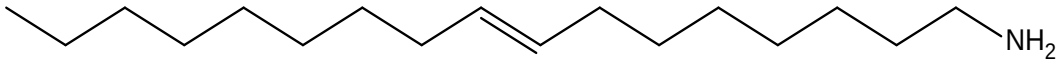

Figure 1.11 Molecular structure of oleylamine.

Thiols

Long chain thiols are a common surfactant and appear to be an excellent capping agent for most semiconducting nanoparticles. In the year 1993, the first report of thiol stabilized CdTe particles appeared, which led to the routine use of the ligand with quantum dots [45]. Medintz has highlighted that monodentate thiol-based capping agents used in biological applications of quantum dots coordinate through dative thiol bonds and are stable for a matter of days. In comparision of monodentate thiols bidentate thiols are, however, much more stable, in the order of years rather than days [46]. Eg. Mercaptoethanol (Figure 1.12) and thiophenol.

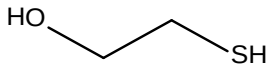

Figure 1.12 Molecular structure of 2-mercaptoethanol.

Carboxylic acids

The use of carboxylic acids as capping agents and surfactants predates the organometallic route by some time. Oleic acid (Figure 1.13) is the standard carboxylic acid used as a surfactant, the double bond and associated ‘kink’ in the alkyl chain are found to be essential features for imparting colloidal stability [47].

The notable difference about the use of carboxylic acids is the fact that they are Lewis acids, unlike the majority of other capping agents which are generally Lewis bases. Zhang et al. reported disklike ZnO microcrystals in presence of citric acid as capping molecules [48].

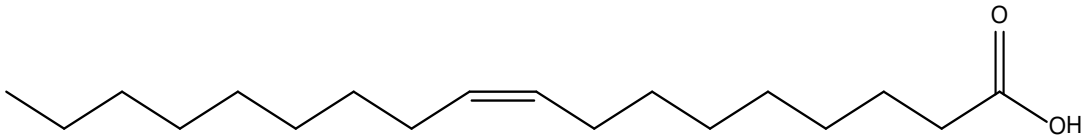

Figure 1.13 Molecular structure of oleic acid.

Polymers

Polymers are also used as capping agents like polyethylene glycol (PEG) (Figure 1.14) [49], polyacrylic acid, polypropylene, polyvinyl alcohol (PVA), Poly(N-vinyl-2-pyrrolidone) (PVP) [50].

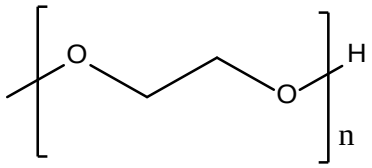

Figure 1.14 Molecular structure of polyethylene glycol.

Surfactants

Surfactants are used as capping agents such as Sodium dodecylsulphate (SDS) (Figure 1.15) [51], cetyltrimethylammonium bromide (CTAB) [52], Triton X-100 [53], cetyltrimetylammonium chloride (CTAC) [54], sodium bis(2-ethylhexyl)sulfosuccinate (AOT) (Figure 1.16) [55]. Surfactants form micelles when dissolved in a solvent. The micelles are used as a nano-reactor.

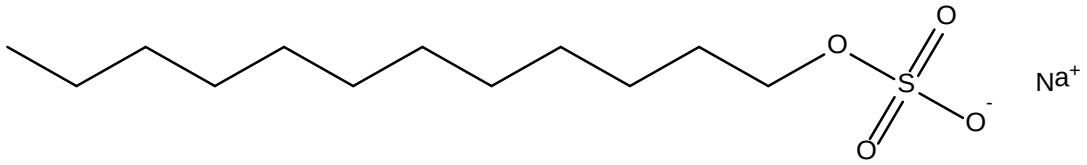

Figure 1.15 Molecular structure of Sodium dodecylsulphate (SDS).

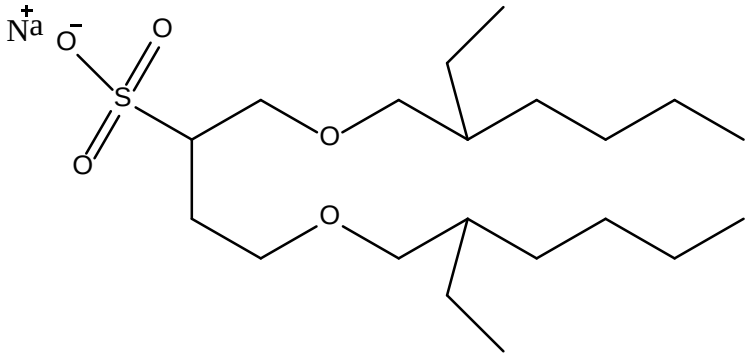

Figure 1.16 Molecular structure of sodium bis(2-ethylhexyl)sulfosuccinate (AOT).

A microemulsion is a thermodynamically stable dispersion of two immiscible fluids and the system is stabilised by added surfactant(s). Different types of microemulsion are known, such as oil-in-water (O/W) and water-in-oil (W/O) dispersions by forming droplet structures called micelles of one phase dispersed within the other. Reverse micelles are formed in a microemulsion which is an isotropic, thermodynamically stable dispersion of water droplets in a continuous oil phase facilitated by a surfactant and/or a cosurfactant.

Some of the advantages of using the microemulsion for nano particle synthesis are given below:

(a) Nanoparticles of a large number of materials can be prepared at room-temperature and pressure.

(b) This technique does not require any sophisticated equipment.

(c) It is possible to control the size and morphology of the particles formed using different experimental parameters such as concentration, temperature etc.

(d) It can be utilized for carrying out different precipitation reactions that are known, to obtain particles in homogeneous solution.

The cosurfactant used is a short chain alcohol or an amine. The aqueous core of a reverse micelle acts as a reactor of nanoscale reaction. When two microemulsions, one containing the metal ion and the other a precipitating agent both in aqueous

solutions, are mixed, the reaction occurs in the aqueous region of the reverse micelle, resulting in the formation of homogeneous and monodispersed nanoparticles. Because of the involvement of several variables (surfactant, cosurfactant, solvent, amount of water, temperature), it is possible to fine-tune the composition of the microemulsion and hence the size and structure of the reverse micelle.

There various factors which affects the growth of particles in reverse micelles such as intermicellar exchange rate [56,57], size, shape, and charge of polar headgroup of surfactant [58, 59], surfactant hydrophobic chain length [60], presence of additives like alcohols, electrolytes, and block copolymers [61], nature of continuous oil phase [62,63] and reactant concentration [64,65].

1.11 ZnS and ZnO nanoparticles

Zinc sulfide, as an important II-VI group semiconductor compound, shows a wide band gap of 3.5-3.7 and 3.7-3.8 eV for sphalerite and wurtzite ZnS, respectively. These bad gap values correspond to the energy range of UV light. ZnS is found in two structural polymorphs—cubic sphalerite or hexagonal wurtzite. Of the two polymorphs, the sphalerite (cubic blende) is considered as the stable phase at standard temperature and pressure. Sphalerite (cubic blende) is a more stable crystal structure than wurtzite below 1020 ºC [66]. In ZnS nanoparticles the phase transformation from the cubic to the wurtzite phase, takes place at relatively low temperature, e.g. temperature 400 ºC for 3 nm ZnS particles [67], due to the high surface energy. ZnS is an attractive candidate for applications in IR windows, and novel photonic devices operating from visible to near-IR region because of the high index of refraction and high optical transmission [68]. The zinc sulfide (bulk) melts at a temperature of 1650°C.

ZnO is one of the most important materials that we come across in our day-to-day lives for example it is used as a pigment in paints and in coating paper ceramics, glass, cement, rubber (e.g. car tyres), lubricants, paints, ointments, adhesives,

sealants, pigments, foods (source of Zn nutrient), batteries, ferrites, fire retardants, etc. ZnO crystallizes in hexagonal wurtzite phase at ambient temperature and pressure. In the earth crust it exists as mineral zincite however, most of commercially used ZnO material is produced synthetically. ZnO finds application in vacuum fluorescent displays (VFD),[69] field emission displays (FED),[70,71] electroluminescent displays (ELD),[72] UV light-emitting diodes (LEDs), and laser diodes [73].

1.12 Doping of transition metal ions into host matrix.

The concept of doping a semiconductor material with atomic impurities is an efficient way to generate luminescent NCs, due to their strong dopant emission. To date, colloidal NCs have successfully been doped with transition metals (such as Fe, Ni, Mn, Cu) and lanthanides (such as Eu, Er, Tm, Tb) to alter their electronic, optical, magnetic or catalytic properties. The band gap of the semiconductor nanocrystals can be tuned between the bulk band gap value and the molecular HOMO-LUMO gap, resulting in a nearly continuous tunability of the band gap over as much as a 2 eV range, which is another advantage. This allows tuning of the excitation energy of the host semiconductor to emit through the dopant levels. When such dopants are introduced in the nanometer-sized ZnS matrix, they show interesting magneto-optical properties [74].

1.13 Optical properties of semiconductor nanoparticles

The optical properties of the nanocrystal can be tailored by judicious control over the particle size and size distribution or by doping with transition metal ions. Photoluminescence (PL) of ZnS doped with different activating metal ions has been extensively investigated in the past few years, due to the tunable PL properties, which have promising applications in optoelectronic devices and LED[75, 76]. Among these doped materials, ZnS NCs doped with Mn^{2+} ions (ZnS: Mn^{2+}) has gained huge interest due to the highly effective luminescence [77].

Figure 1.17 Energy-level diagram showing some of the energy changes that occur during absorption, nonradiative relaxation, and fluorescence by molecular species [78].

In photoluminescence spectroscopy, the emission of photons is measured after absorption and important forms of photoluminescence are fluorescence and phosphorescence spectroscopy [78]. Fluorescence is a photoluminescence process in which atoms and molecules are excited to higher energy lavel by absorption of electromagnetic radiation, as shown in Figure 1.17. The excited species, relax back to ground state, giving undoped excess energy in the form of photons. Nonradiative relaxation and fluorescence emission are the two of the most important mechanisms.

In the nonradiative relaxation, two types of relaxations occur such as vibration relaxation or deactivation which takes place during collisions between excited molecules and molecules of the solvent. Non radiative relaxation between the lowest vibrational level of an excited electronic state can occur, which is known as internal

conversion. Different bands of radiation are produced when molecules relax from the lowest lying vibrational state of an excited state E_1 to the many vibrational levels of the ground state E_0. The transition from E_1 to the lowest lying vibrational state of the ground state (λ_1) has the highest energy in comparision with all other transitions in the band. As a result, all the other lines that terminate in higher vibrational levels of the ground state are lower in energy and hence produce fluorescence emission at longer wavelengths than λ_1. The molecular fluorescence bands consist of lines, which are longer in wavelength than the band of absorbed radiation responsible for their excitation. This shift in wavelength is known as the Strokes shift.

ZnS as a host material itself shows blue luminescence but on Mn doping a red shift occurs and a new orange luminescence appears due to $^4T_1$ - $^6A_1$ transition via energy transfer from ZnS host [79]. The orange luminescence of Mn doped ZnS can be well represented by Figure 1.18 [80].

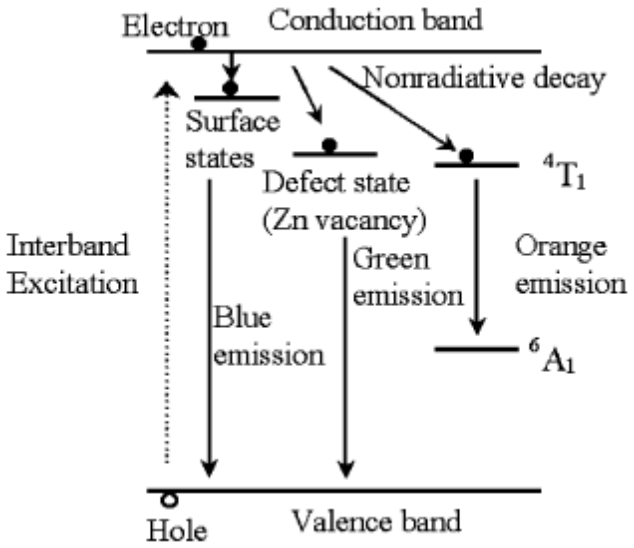

Figure. 1.18 Schematic representation of the model ascribed to different emission from the $Mn_xZn_{1-x}S$ nanorods [80].

In photoluminescence (PL) studies, a more satisfying description of a physical system should include a treatment of lifetimes as well. In case of semiconducting materials, some of the 3d transition elements play the role of substitutional impurities and

participate in the luminescence kinetics as ‘killers’. To investigate the mechanisms of this usually undesirable yet important effect, which is related to non-radiative recombination, knowledge of radiative transition probabilities would also be helpful. The radiative relaxation phenomena include free-to-bound and pair recombination processes and not the internal transitions of the activator ions. For the most of 3d transition elements, the lifetimes of the excited states at nanoscale are largely unknown, which needs to be further studied.

1.14 Electrical properties

Now days, efforts are made to construct hetero structures on the surface of silicones. For example, ZnS is allowed to grow on the Si surface, for some time then ZnO will continue the growth process resulting into ZnS/ZnO core-shell or hetero structured nano wires or belts. In the same line of work, Lu, Y et al synthesized ZnO-ZnS hetero junction nanowire arrays by thermal evaporation in a tube furnace under controlled conditions [81]. They also converted these hetero junctions into pure ZnS nanowires arrays by etching process. They found that both types of materials were piezoelectric in nature and could be used to generate electric power under mechanical stress (of AFM tip, in this case). Such types of complex structures might show novel applications such as three terminal ballistic junctions or Y-branched junctions [82, 83], optical pumped lasers [84] etc. Thus, nanostructured materials open door to new functional materials and hence devices.

Nanosized particles of semi conducting compounds in particular display grain size dependent optoelectronic properties because the size quantization effects [85]. In photovoltaic devices, nanoparticles are mixed with a conjugated polymer and the process of charge transfer from polymer and transport in nanoparticles is critical to their operation [86].

The dielectric constant of nanomaterials should be larger than that of the conventional materials due to sufficiently high temperature, increased space charge polarization due to the structure of their grain boundary interfaces [87].

The electrical property study of samples indicated the conductivity enhancement from 2.981×10-6 to 7.014 ×10-6 S/m by increasing PVP concentration [88].The electrical resistivity data of ZnS and Ni doped ZnS nanoparticles reveals semiconducting behavior [89]. Cu when added as a dopant ion behaves as an acceptor in ZnO with its energy level locating at 0.17 eV below the bottom of the conduction band, making itself a good candidate for creating p-type ZnO [90].

1.15 Magnetic properties

One method of making a semiconductor magnetic is to lightly dope it with magnetic impurities like transition metal ions, resulting in the so-called diluted magnetic semiconductors (DMS) [91]. It has attracted intense interest in the field of spin-based electronics, or “spintronics”[92,93] .

DMS materials have interesting magnetotransport and magneto-optical properties due to the presence of localized magnetic ions and the consequent large sp-d exchange interaction, resulting in extreme Zeeman splittings of electronic levels [94]. Among them, ZnO doped with 3d transition metal ions (Mn, Fe, Co, or Ni) has been particularly studied, because it was predicted to exhibit ferromagnetic ordering (FM) at room temperature (RT) [95].

1.16 Catalytic activity

High surface to volume ratio makes them suitable for catalysis and/or photocatalytic applications. An ideal photocatalyst should be stable, inexpensive, non-toxic and, of course, highly photocatalytically active. Another basic criterion for the degradation of organic compounds is that the redox potential of the $H_2O/\cdot OH$ couple ($OH^- \rightarrow \cdot OH + e^-$; Eo = −2.8 V) lies within the bandgap of the semiconductor [96].

Photocatalysis using Semiconductor offers the potential for complete elimination of toxic chemicals through its efficiency and potentially broad applicability [97]. Now-a-days transition-metal sulfides, in particular ZnS and CdS, have been intensively studied because of their unique catalytic functions compared to those of TiO_2 [98]. These studies have revealed that ZnS nanocrystals (NCs) are good photocatalysts because of the rapid generation of electron-hole pairs by photoexcitation and the highly negative reduction potentials of excited electrons.

Dyes are used by industries on a vast scale. These dyes are non-biodegradable which causes pollution. Waste water from textile, paper and some other industries contain residual dyes, which are not readily biodegradable, reach the water streams which causes pollution. Due to environmental issues dyes should be removed. These dyes represent a significant environmental hazard to aquatic biota and humans due to their toxicity and tendency to cause eutrophication. Improvements in chemical structure have led to increased longevity of dyed fabrics as a consequence make the textile wastewater more difficult to treat. This effluent requires appropriate treatment before it is discharged to the environment because the colour and toxicity caused by these dyestuffs may have a detrimental impact on water quality. The use of semiconductor material as a photocatalyst for the dye degradation has gained interest in the past few years.

When semiconductor particles absorb light, electrons are promoted from the valence band of the particle to its conduction band, delocalized electron-hole pairs, or

excitons are generated. The gap between valence and conduction bands is very small, and the electrons and holes can recombine efficiently in bulk particles. In nanoparticles the band gap increases due to quantum confinement effects and the charge separation between the hole and the electron becomes pronounced. A high surface to volume ratio insures that electrons and holes have ready surface access in comparision with the bulk material, thereby enhancing their photocatalytic action for efficient oxidation and reduction processes [99].

A basic mechanism of photocatalytic reaction on the generation of electron–hole pair and its destination is as follows: when photocatalyst particles absorb light, electrons are promoted from the valence band of the particle to its conduction band, delocalized electron-hole pairs, or excitons are generated, that diffuse out to the surface of the photocatalyst and participate in the chemical reaction with the electron donor and acceptor. These free electrons and holes transform the surrounding oxygen or water molecules into OH· free radicals with super strong oxidization [100].

1.17 Biological Applications

ZnO has been extensively used as an inorganic antibacterial reagent in the food industry, due to its stability, better antibacterial activity and it is safe to human beings and animals [101]. Toxicological studies carried out in the past few years showed that ultrafine particles ($d < 100$ nm) pose serious problems to the lungs [102]. It was reported that these nanoparticles cause more inflammation than larger respirable particles made from the same material when delivered at the same mass dose.
The quantum dots are used in the cellular imaging. It offers high brightness and sensitivity along with advantage of availability of a large number of well-separated colors, all excitable with one single source.[103,104]

One major drawback that severely limits the use of II–VI semiconductor QDs (such as CdSe and CdTe) in various biomedical applications [105], particularly in the light of recent environmental regulations, is their toxicity. This toxicity results mainly from

decomposition and release of heavy metal ions and formation of highly reactive oxygen species [106-110] during its application. Therefore, in recent years, the emphasis has shifted toward the fabrication of non-cadmium-based QDs for applications in the field of biology.

However, ZnS and ZnO nanoparticles are very suitable for applications in biological fields due to less toxicity among other II–VI semiconductor nanoparticles. Doped-ZnS QDs are extremely promising candidates as they are not only cadmium-free but also show stable luminescence and high quantum efficiency [111-113] which is the required properties. ZnS is also particularly suitable as a host material for a large variety of dopants due to its wide band gap (3.67 eV).

ZnO NPs have been widely used in products where UV protection from a transparent coating is required, such as in varnishes to protect wood and in the cosmetics as sunscreens to protect skin. The extremely small size of NPs increases the possibility of their uptake by cells and interactions with biological molecules and tissues, thereby providing advantageous opportunities but at the same time potential risks for their application. Some of the recent studies have shown that ZnO NPs can be toxic to a wide variety of biological systems, including epidermal cells, [114] bacteria (Streptococcus agalactiae and Staphylococcus aureus), [115] zebra fish (Danio rerio), [116] and mice [117].

1.18 Aim and Scope of the Present investigation

The aim of the study was to develop an easy method to synthesize various transition metals doped and undoped ZnS nanoparticles. The main objectives were:

- To optimize the solvent/surfactant ratio for above mentioned methods and to study the effect of such ratio on the shape of nanoparticles.

- To study the effect of various surface modifiers on the photoluminescence properties of II-VI semiconductor nanoparticles systems and to optimize the host to dopant ratio for having excellent quantum yield.

- To study the effect of size reduction, as well as effect of various transition metals as dopant, on the electrical behavior on ZnS.

- These materials also behave as Diluted Magnetic Semiconductor (DMS) and have applications in spintronics. So the effect of size and shape of nanoparticles on such properties are studied.

- To study the change in size and shape of the nanomaterial. The mechanism of shape change on entrapment in host matrix is still not clear. Therefore, it will be worth exploring. The effect of such changes will be studied in terms of electrical, optical and magnetic response of the material.

1.19 Characterization

X-ray Powder diffraction (XRD) patterns of samples were obtained by a Guinier X-ray Powder diffraction diffractometer (Bruker D8) with Cu Kα radiation, λ=0.15418 nm. Transmission Electron Microscopy (TEM, Philips Tecnai 20) and high resolution scanning electron microscopy (HRSEM, Quanta 200 FEG) were employed to confirm the size and morphology of the nanoparticles. The samples were degassed at 80 °C prior to BET measurements. The Brunauer-Emmett-Teller (BET) specific surface area (SBET) was determined by nitrogen adsorption in a Micrometrics ASAP2020 nitrogen adsorption apparatus (USA) via a multipoint BET method using the adsorption data in the relative pressure (P/Po) range of 0.0 -1.0. The desorption isotherm was used to determine the pore-size distribution using the Barret-Joyner-Halender (BJH) method, assuming a cylindrical pore model. The nitrogen adsorption volume at the relative pressure (P/Po) range of 0.997 was used to determine the pore volume and average pore size. The compositional analysis of the powder samples were carried out using Energy Dispersive X-ray analyses (EDX) (JEOL 8086). The solid samples were dispersed in water and sonicated for 10 minutes to record UV-visible absorption (Perkin Elmer Lamda 35) and photoluminescence (Jasco FP-6300) spectra at room temperature. Photoluminescence (PL) spectra were recorded using Xenon lamp as the excitation source at 290 nm. A BIC 90 plus (Brookhaven) equipped with 35.0 mW solid state lasers operating at 660 nm and an avalanche photodiode detector was used for the measurement of surface charges in terms of zeta potential. All measurements were made at 25°C in DI water. Inductive coupled plasma atomic emission spectroscopy (ICP-AES) was recorded using Perkin-Elmer Optima 3300 RL. Differential scanning calorimetric (DSC) analysis was carried out using Mettler Toledo DSC 822. For the purpose, the material is heated inside a DSC set-up. The heating rate was 10 ºC/min from RT to 500 ºC in N_2 atmosphere.

The Mössbauer spectra were recorded in the transmission geometry with a constant acceleration transducer and a 512 channel multichannel analyzer. A 57Co (Rh) source of activity 10 m Ci was used. The line width of the spectrometer was 0.27 mm/sec.

The solid lines through the data points are the results of computer fit of the data. Magnetic hysteresis [M(H)] curves were obtained by Vibrating Sample Magnetometer (VSM) measurements at 300 K on Lakeshore VSM 7410. The Mott-Schottky study was performed using an Electrochemical Analyser (CHI660E, CH instruments, Inc., Austin, USA). The semiconductor on ITO glass was used as working electrode. The ITO glass was degreased by surfactant for 10 min, followed by distilled water and last alcohol rinse for 10 min in an ultrasonic bath. Then ZnS nanoparticles with or without Fe dopant were dispersed in organic polar solvent (EtOH: DMSO, 1: 0.2). The solution was spin-coated on the clean substrates at 3500 rpm for 30 sec, and spin coated film put at 50˚C for 20 min in oven. The Ag/AgCl electrode and platinum wire were used as reference and counter electrodes, respectively.

References

[1] There is Plenty of Room at the Bottom, R. Feynman in The Pleasure of Finding Things Out, (Ed.: J. Robbins), Perseus Books, **1999**.

[2] H. Goesmann, C. Feldmann *Angew. Chem. Int. Ed.* **2010**, 49, 1362.

[3] M.D. Morse, *Chem. Rev.* **1986**, 86, 1049.

[4] A. Henglein, *Chem. Rev.* **1989**, 89, 1861.

[5] *Future Trends in Microelectronics: The Nano Millennium* (Eds: S. Luryi, J. Xu, A. Zaslavsky), Wiley-Interscience, New York **2002**.

[6] N. Shiju, G. Raveendran, V. Vadim, *Appl. Catal. A* **2009**, 356, 1.

[7] W. Umbach, *Kosmetik-Entwicklung, Herstellung und Anwendung kosmetischer Mittel*, Wiley-VCH,Weinheim, **1995**, p. 147.

[8] H.C. van de Hulst, *Light Scattering by Small Particles*, Dover Publications, New York, **1981**.

[9] J. Stangl, V. Holy, G. Bauer, *Rev. Mod. Phys.* **2004**, 76, 725.

[10] M.L. Steigerwald, LE. Brus, *Acc. Chem. Res.* **1990**, 23, 183.

[11] H. Haug, S. W. Koch, *Quantum theory of the Optical and Electronic Properties of Semiconductors*, World Scientific Publishing Co. Pte. Ltd., London, **1990**, p 333.

[12] L.E. Brus, *J. Chem. Phys.* **1983**, 79, 5566.

[13] L.E. Brus, *J. Chem. Phys.* **1984**, 80, 4403.

[14] L. Brus, *J. Phys. Chem.* **1986**, 90, 2555.

[15] A.N. Goldstein, C.M. Echer, A.P. Alivisatos, *Science* **1992**, 256, 1425.

[16] C.S. Tiwary, C. Srivastava, P. Kumbhakar, *J. Appl. Phys.* **2011**, 110, 034908.

[17] W. Vogel, J. Urban, M. Kundu, S. K. Kulkarni, *Langmuir* **1997**, 13, 827−830.

[18] X.H. Liao, J.J. Zhu, H.Y. Chen, *Mater. Sci. Eng. B* **2001**, 85, 85.

[19] F. Huang, J.F. Banfield, *J. Am. Chem. Soc.* **2005**, 127, 4523.

[20] N.I. Kovtyukhova, E.V. Buzaneva, C.C. Waraksa, T.E. Mallouk, *Mater. Sci. Eng. B* **2000**, 69/70, 411.

[21] Q. Zhao, L. Hours, R. Huang, *Inorg. Chem. Commun.* **2003,** 6, 971.

[22] J.H. Bang, R.J. Helmich, K.S. Suslick, *Adv. Mater.* **2008,** 20, 2599.

[23] Q.J. Feng, D.Z. Shen, J.Y. Zhang, H.W. Liang, D.X. Zhao, Y.M. Lu, X. W. Fan, *J. Cryst. Growth* **2005,** 285, 561.

[24] Y. Yang, Y. Chu, F.Y. Yang, Y.P. Zhang, *Mater. Chem. Phys.* **2005,** 92, 164.

[25] F.Y. Yang, Y. Chu, L. Huo, Y. Yang, Y. Liu, *Chem. Lett.* **2005,** 34, 388.

[26] P.V. Braun, S.L. Stupp, *Mater. Res. Bull.* **1999,** 34, 463.

[27] D. Lootens, C. Vautrin, H.V. Damme, T. Zemb, *J. Mater. Chem.* 13 (**2003**) 2072.

[28] Y.R. Ma, L.M. Qi, J.M. Ma, H.M. Cheng, W. Shen, *Langmuir* 19 (**2003**) 9079.

[29] J. Jang, K. Lee, *Chem. Commun.* (**2002**) 1098.

[30] Y. Yin, A. P. Alivisatos, *Nature* **2005**, 437, 664.

[31] S.F.Wuister, C. de Mello Donegá, A. Meijerink, J. Phys. Chem. B, **2004**, 108, 17393.

[32] T. Teranishi, Y. Inoue, M. Nakaya, Y. Oumi, T. Sano, *J. Am. Chem. Soc.*, **2004**, 126, 9914.

[33] T. Kubo, T. Isobe, M. Senna *J. of Luminescence* **2002,** 99, 39.

[34] C.B. Murray, D.J. Norris, M.G. Bawendi, *J. Am. Chem. Soc.*, **1993**, 115, 8706.

[35] S. Sun, C.B. Murray, J. Appl. Phys., **1999**, 85, 4325.

[36] A. Hoshino, K. Fujioka, T. Oku, M. Suga, Y.F. Sasaki, T. Ohta, M. Yasuhara, K. Suzuki, K. Yamamoto, *Nano Lett.*, **2004**, 4, 2163.

[37] O.I. Mićić, J.R. Sprague, C.J. Curtis, K.M. Jones, J.L. Machol, A.J. Nozik, H. Giessen, B. Fluegel, G. Mohs, N. Peyghambarian, *J. Phys. Chem.*, **1995**, 99, 7754.

[38] M. Furis, Y. Sahoo, D.J. MacRae, F. S. Manciu, A.N. Cartwright, P.N. Prasad, *J. Phys. Chem. B* **2003**, 107, 11622.

[39] D.V. Talapin, A.L. Rogach, I. Mekis, S. Haubold, A. Kornowski, M. Haase and H. Weller, *Colloids Surf. A*, **2002**, 202, 145.

[40] D.V. Talapin, A.L. Rogach, A. Kornowski, M. Haase, H. Weller, *Nano Lett.*, **2001**, 1, 207.

[41] W.K. Woo, PhD thesis, MIT, **2002**.

[42] R. Li, J. Lee, B. Yang, D.N. Horspool, M. Aindow, F. Papadimitrakopoulos, *J. Am. Chem. Soc.* **2005**, 127, 2524.

[43] J.-Y. Zhang, X.-Y. Wang, M. Xao, L. Qu, X. Peng, *Appl. Phys. Lett.* **2002**, 81, 2076.

[44] G. Kremser, The Rath, B. Kunert, M. Edler, G. Fritz-Popovski, R. Resel, I. Letofsky-Papst, W. Grogger, G. Trimmel, *J. Colloid Interface Sci.* **2012**, 369, 154.

[45] T. Rajh, O. I. Mićić, A. J. Nozik, *J. Phys. Chem.* **1993**, 97, 11999.

[46] I.L. Medintz, H. Tetsuo Uyeda, E.R. Goldman, H. Mattoussi, *Nat. Mater.* **2005**, 4, 435.

[47] R. Tadmor, R.E. Rosensweig, J. Frey, J. Klein *Langmuir* **2000**, 16, 9117.

[48] H. Zhang, D. Yang, D. Li, X. Ma, S. Li, D. Que *Cryst. Growth Des.* **2005**, 5, 547.

[49] L. Dong, Y. Chu, Y. Zhang, Y. Liu, F. Yang *J. Colloid Interface Sci.* **2007,** 308, 258.

[50] S. K. Panda, A. Datta, S. Chaudhuri, *Chemical Physics Letters* **2007**, 440, 235.

[51] R. Mitra, I. Charaborty, S. P. Moulik, *Colloid J.* **2005,** 67, 494.

[52] A. Murugadoss, A. Chattopadhyay, *Bull. Mater. Sci.* **2008,** 31, 533.

[53] J. Xu, Y. Li, *J. Colloid Interface Sci.* **2003,** 259, 275.

[54] S. K. Mehta, S. Kumar, S. Chaudhary, K. K. Bhasin *Nanoscale Res Lett* **2009**, 4, 1197.

[55] F. Li, Y. Ding, P. Gao, X. Xin, Z.L. Wang, *Angew. Chem. Int. Ed.* **2004**, 43, 5238-5242.

[56] J. Eastoe, D. Sharpe, *Langmuir* **1997**, 13, 3289.

[57] T. Ahmad, R. Chopra, K.V. Ramanujachary, S.E. Lofland, A.K. Ganguli, *Solid State Sci.* **2005**, 7, 891.

[58] J.P. Cason, M.E. Miller, J.B. Thompson, C.B. Roberts, *J. Phys. Chem. B* **2001**, 105, 2297.

[59] M.A. Quintela, *Curr. Opin. Colloid Interface Sci.* **2003**, 8, 137.

[60] I. Capek, *Adv. Colloid Interface Sci.* **2004**, 110, 49.

[61] J.P. Cason, M.E. Miller, J.B. Thompson, C.B. Roberts, *J. Phys. Chem. B* **2001**, 105,2297.

[62] J. Eastoe, D. Sharpe, *Langmuir* **1997**, 13, 3289.

[63] S. Vaidya, P. Rastogi, S. Agarwal, S.K. Gupta, T. Ahmad, A. Antonelli, K.V. Ramanujachary, S. E. Lofland, A. K. Ganguli, *J. Phys. Chem. C* **2008**, 112, 12610.

[64] A. Filankembo, S. Giorgio, I. Lisiecki, M. P. Pileni, *J. Phys. Chem. B* **2003**, 107, 7492.

[65] A. Filankembo, M.P. Pileni, *J. Phys. Chem. B* **2000**, 104, 5865.

[66] L. Yin,Y. Bando *Nat. Mater.* **2005**, 4, 883.

[67] S.B. Qadri, E. F. Skelton, D. Hsu, A.D. Dinsmore, J. Yang, H.F. Gray, B.R. Ratna, *Phys. Rev. B* **1999,** 60, 9191.

[68] Y. Yamada, K. Yoshimura, S. Fujita, T. Taguchi, *Appl. Phys. Lett.* **1997**, 70, 1429.

[69] S. Ruan, *Proc. SPIE-Int. Soc. Opt. Eng.* **1996**, 262, 2892.

[70] Y. Nakanishi, A. Miyake, H. Kominami, T. Aoki, Y. Hatanaka, G. Shimaoka, *Appl. Surf. Sci.* **1999**, 142, 233.

[71] S. Fujihara, Y. Ogawa, A. Kasai, *Chem. Mater.* **2004**, 16, 2965.

[72] L. Yi, Y. Hou, H. Zhao, D. He, Z. Xu, Y. Wang, X. Xu, *Displays* 2000, 21, 147 149.

[73] R.F. Service, *Science* **1997**, 276, 895.

[74] T.A. Kennedy, E.R. Glaser, P.B. Klien, R.N. Bhargava, *Phys. Rev. B* **1995**, 52, 14356.

[75] H.S. Yang, P.H. Holloway, B.B. Ratna, *J. Appl. Phys.* **2003**, 93, 586.

[76] J.P. Ge, J.W. Wang, H.X. Zhang, X. Wang, Q. Peng, Y.D. Li, *Adv. Funct. Mater.* **2005**, 15, 303.

[77] R.H. Bhargava, D. Gallagher, *Phys. Rev. Lett.* **1994**, 72, 416.

[78] D.A. Skoog, D.M. West, F.J. Holler, S. R. Crouch, *Fundamentals of Analytical Chemistry*, **2009**.

[79] L.M. Gan, B. Liu, C.H. Chew, S.J. Xu, S.J. Chua, G.L. Loy, G.Q. Xu, *Langmuir* 1997, 13, 6427.

[80] S. Biswas, S. Kar, S. Chaudhuri, *J. Phys. Chem. B* **2005**, 109, 17526.

[81] L.E. Brus, *J. Chem. Phys.* **1984,** 80, 4403.

[82] X. Peng, *Acc. Chem. Res.* **2010,** 43, 1387.

[83] L.M. Gan, B. Liu, C.H. Chew, S.J. Xu, S.J. Chua, G.L. Loy, G.Q. Xu, *Langmuir* **1997**, 13, 6427.

[84] H. Ohno, *Science* **1998,** 281, 951.

[85] M. Bangal, S. Ashtaputre, S. Marathe, A. Ethiraj, N. Hebalkar, S.W. Gosavi, J. Urban, S.K. Kulkarni, *Hyperfine Interact.* **2005**, 160, 81.

[86] C.E. Finlayson, D.S. Ginger, E. Marx, N.C. Greenham, *Phil. Trans. R. Soc. Lond. A* **2003**, 361, 363.

[87] J. Meera, V. Sumithra, R. Seethu, J.M. Prajeshkumar, *Acad. Rev.* **2010,** 1, 93.

[88] N. Soltani, A. Dehzangi, A. Kharazmi, E. Saion, W.M.M. Yunus, B.Y. Majlis, M.R. Zare, E. Gharibshahi, N. Khalilzadeh, *Chalcogenide Letters* **2014,** 11, 79.

[89] A. Firdous, *Eur. Phys. J. Appl. Phys.* **2010,** 52, 20602 p-1-5.

[90] Kanai, Y. *Jpn. J. Appl. Phys.* **1991**, 30, 703.

[91] Furdyna, J. K. *J. Appl. Phys.* **1988**, 64, R29.

[92] H. Ohno, D. Chiba, F. Matsukura, T. Omiya, E. Abe, T. Dietl, Y. Ohno, K. Ohtani, *Nature* **2000**, 408, 944.

[93] Y. Ohno, D.K. Young, B. Beschoten, F. Matsukura, H. Ohno, D.D. Awschalom, *Nature* **1999**, 402, 790.

[94] J.K. Furdyna, *J. Appl. Phys.* **1988,** 64, R29**.**

[95] T. Dietl, H. Ohno, F. Matsukura, J. Cibert, D. Ferrand, *Science* **2000**, 287, 1019.

[96] H. Al-Ekabia, N. Serpone, *J. Phys. Chem.* **1988**, 92, 726.

[97] M.R. Hoffmann, S.T. Martin, W. Choi, D.W. Bahnemann, *Chem. Rev.* **1995**, 95, 69.

[98] S. Yanagida, K. Mizumoto, C.J. Pac, *J. Am. Chem. Soc.* **1986**, 108, 647.

[99] D. Beydoun, R. Amal, G. Low, S. McEvoy, *J. Nanoparticle Res.* **1999**, 1, 439.

[100] Y.J. Jang, C. Simer, T. Ohm, *Mater. Res. Bull.* **2006,** 41, 67.

[101] K. Reddy, K. Feris, J. Bell, D. Wingett, C. Hanley, A. Punnoose, *Appl. Phys. Lett.*, **2007**, 90, 213902.

[102] K. Donaldson, V. Stone, A. Clouter, L. Renwick, W. Macnee, *Occup. Environ. Med.* **2001**, 58, 211.

[103] A.M. Smith, S. Dave, S.M. Nie, L. True, X.H. Gao, *Expert Rev. Mol. Diagn.* **2006**, 6, 231.

[104] I.L. Medintz, H.T. Uyeda, E.R. Goldman, H. Mattoussi, *Nat. Mater.* **2005**, 4, 435.

[105] S.J. Klaine, P.J.J. Alvarez, G.E. Batley, T.F. Fernandes, R.D. Handy, D.Y. Lyon, *Environ Toxicol Chem* **2008**, 27,1825.

[106] C. Kirchner, T. Liedl, S. Kudera, T. Pellegrino, A.M. Javier, H.E. Gaub, *Nano Lett* **2005**, 5, 331.

[107] Y. Zhang, J. He, P.N. Wang, J.Y. Chen, Z.J. Lu, D.R. Lu, *J. Am. Chem. Soc.* **2006**, 128, 13396.

[108] J. Ma, J.-Y. Chen, Y. Zhang, P.-N. Wang, J. Guo, W.-L. Yang, *J Phys Chem B* **2007**, 111, 12012.

[109] Z. Lu, C.M. Li, H. Bao, Y. Qiao, Y. Toh, X. Yang *Langmuir* **2008**, 24, 5445.

[110] R. Schneider, C. Wolpert, H. Guilloteau, L. Balan, J. Lambert, C. Merlin, *Nanotechnology* **2009**, 20, 225101.

[111] R. Thakar, Y.C. Chen, P.T. Snee, *Nano Lett.* **2007**, 7, 3429.

[112] D. J. Norris, A.L. Efros, S. C. Erwin, *Science* **2008**, 319, 1776.

[113] H. Hu, W. Zhang, *Opt. Mater.* **2006**, 28, 536.

[114] V. Sharma, R.K. Shukla, N. Saxena, D. Parmar, M. Das, A. Dhawan, *Toxicol. Lett.* **2009**, 185, 211.

[115] Z.B. Huang, X. Zheng, D.H. Yan, G.F. Yin, X.M. Liao, Y.Q. Kang, Y.D. Yao, D. Huang, B.Q. Hao, *Langmuir* **2008**, 24, 4140.

[116] X.S. Zhu, L. Zhu, Z.H. Duan, R.Q. Qi, Y. Li, Y.P. Lang, *J. Environ. Sci. Health, Part A: Environ. Sci. Eng.* **2008**, 43, 278.

[117] B. Wang, W.Y. Feng, M. Wang, T.C. Wang, Y.Q. Gu, M.T. Zhu, H. Ouyang, J.W. Shi, F. Zhang, Y.L. Zhao, Z.F. Zhai, H.F. Wang, J. Wang, *J. Nanopart. Res.* **2008**, 10, 263.